USE OF MODAL REPRESENTATION FOR THE SUPPORTING STRUCTURE IN MODEL BASED FAULT IDENTIFICATION OF LARGE ROTATING MACHINERY: PART 2 – APPLICATION TO A REAL MACHINE

NICOLÒ BACHSCHMID, PAOLO PENNACCHI, ANDREA VANIA

Dipartimento Di Meccanica,
Politecnico di Milano,
Via La Masa 34, I-20156 Milano
nicolo.bachschmid@polimi.it,andrea.vania@polimi.it, paolo.pennacchi@polimi.it

GIAN ANTONIO ZANETTA, LUCA GREGORI

Area Generazione,
CESI-S.p.A.,
Via Reggio Emilia 39, I-20090 Segrate (MI), Italy
zanetta@cesi.it, lgregori@cesi.it

Please send proofs to
PROF. PAOLO PENNACCHI
Dipartimento Di Meccanica,
Politecnico di Milano,
Via La Masa 34, I-20156 Milano

ABSTRACT

Model based techniques are often employed in diagnostics of rotating machines to locate and to evaluate the severity of the malfunction. The use of a reliable model can increase the accuracy of the identification. Rigid supports or lumped mass pedestals are not always enough to account for the foundation dynamics; a modal representation of the supports can improve the identification results. The method, discussed in the first part is here validated using experimental data of a 320 MW steam turbogenerator. At the authors' knowledge, this is the first case of fault identification on real data from a large machine, where the supporting structure is accounted for by means of a modal model.

1 INTRODUCTION

Among the many different topics of concern in the rotordynamics, the prompt identification of faulty conditions is for sure a prominent one. Early diagnosis reduces off-line times of unexpected outages, allows the implementation of predictive maintenance policies, makes it possible to predict residual life and it prevents dangerous accidents and break-downs.

In the rotordynamics field different techniques are used for identification purposes [1-8]. Anyhow, when the identification task is to locate the fault along the rotor train and to evaluate the severity of the malfunction, model based techniques, both in frequency and in time domain, are often preferred [9-10].

The fault identification technique proposed by the authors [11, 12], based on a least square algorithm in frequency domain, has proven to be quite robust in general, even if the whole system model was not necessarily fine tuned, in large rotating machines where the foundation was modelled by means of pedestals. Of course, the use of a reliable model can increase the accuracy of the identification. In case of machines in which foundation resonances span over a large range of rotating speeds, an equivalent modal model is the easiest and most immediate way to account for the foundation dynamics and the relevant theory has been introduced in the first part of the paper.

Modal identification techniques applied to the rotating machinery foundations and exploiting data collected during the normal operation of the machine, rather than data obtained by cumbersome and costly modal tests, are proposed by several authors [13-16]. As it has been discussed in the first part of the paper, a modal model of the foundation provides in any case some more degrees of freedom for improving the tuning of the complete system model and the subsequent least-squares identification quality.

In this second part of the paper, the effectiveness of the method is proven using experimental results obtained by processing real data obtained from an in-situ trim balancing test on a 320 MW steam turbogenerator set.

2 MODEL OF A 320MW STEAM TURBOGENERATOR SET

The application of the concepts introduced in paragraph 3.1 and 3.2 is presented by means of an experimental case of 320MW steam turbogenerator. This machine started its operations

more than 10 years ago in a plant where three similar machines were already installed, at that time operated by a primary Italian utility.

The rotor train was supported on seven journal bearings (see figure 1). The rotating machine was composed of an high-intermediate-pressure (HP-IP) turbine, a low-pressure (LP) turbine and a generator, coupled by rigid joints. It had the gross mass of approximately of 111 t and the length of 28.4 m. The turbogenerator was supported on a concrete top plate supported on eight pilasters which were connected to a base plate supported on the sub-soil. Spring elements were mounted between the top-plate and the pilasters. They significantly affected the dynamic behaviour of the foundation. The concrete top plate showed some large holes in order to allow the link between the turbogenerator and some machine components located under the plate.

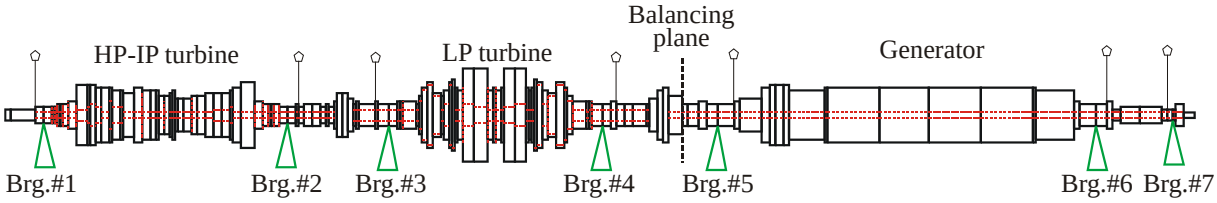

Figure 1 320MW steam turbogenerator model.

At each lubricated journal bearing the shaft vibrations relative to the bearing housing were measured with a couple of X-Y proximity probes while the absolute vibrations of the supports were measured with a couple of X-Y velocimeters. A condition monitoring system collected the vibration data associated to these measurement points (overall amplitude, 1x rev., 2x rev. and 3x rev. harmonic components) both in running state and in transient state (runups and rundowns).

The vibration data collected during several run-ups and run-downs were available. During the monitoring period that has been considered, a trim balancing operation was carried out: a balancing mass was positioned at the rigid coupling located between the low-pressure turbine and the generator in order to reduce the levels of the relative vibrations measured at the generator bearing #5. Since our purpose is to identify a faulty condition and a real turbogenerator is not a test-rig in which an unbalance is simply made by inserting some screws in holes of disks, without loosing of generality, the actual operating conditions are reversed. The run-down before the balancing is considered as the reference condition and the run-down after the balancing as the faulty condition. This way, under the hypothesis of

linearity of the system, which is rather true for this specific type of machines as discussed in [11,12,17], it is possible to evaluate additional vibrations due to an unbalance of known location and amount. Since the fault considered is the unbalance, only 1x rev. additional vibration are considered.

2.1 Machine model definition

2.1.1 Rotor model

The rotor train model, shown in figure 1, has 162 finite beam elements, of which 70 for the HP-IP turbine, 60 for the LP turbine and 32 for the generator. The model of the rotor itself is in general quite reliable and the sensitivity analysis performed by rotordynamics codes [17] shows that, at least for this kind of machines, the uncertainties in the shaft and mass diameters of the rotor have a secondary effect on the critical speed and modal damping values with respect to bearing and support characteristics. The rotor model is considered to be reliable since the other machines of the same type are installed in the same plant and in other plants and a rather intense tuning on these machines was performed. In regards to the measuring planes, in this case they are not located in the same nodes of the bearing, but in the nodes immediately close, as shown in figure 1 and table 1.

Table 1 Measuring planes offsets from bearings.

	Measuring plane #1	Measuring plane #2	Measuring plane #3	Measuring plane #4	Measuring plane #5	Measuring plane #6	Measuring plane #7
Offset from bearing [mm]	–241	+229	–286	+286	–195	+195	–80

2.1.2 Bearing models

As for the stiffness and damping linearized coefficients of the seven bearings, of which #1, #2 are equal and of tilting pad type, #3 and #4 equal and elliptical, #5 and #6 equal and elliptical and the last #7 of tilting pad type, the values taken from tables in the published literature [18] were first assigned. These starting values were then modified in the attempt to tune the whole system model to the experimental data and are shown from **Errore. L'origine riferimento non è stata trovata.** to **Errore. L'origine riferimento non è stata trovata.**.

Since the actual alignment conditions of the specific machine can strongly influence the oil-film forces, they could not be actually equal two by two. The estimation of the actual

linearized coefficient of the machine analyzed would require a more fine tuning, therefore they must be considered as fair.

Table 2 Linearized dynamic coefficents for bearing #1 & #2.

Rotating speed	k_{xx}	k_{xy}	k_{yx}	k_{yy}	r_{xx}	r_{xy}	r_{yx}	r_{yy}
300	2.00e9	0	0	2.00e9	2.00e8	0	0	2.00e8
1000	1.20e9	0	0	1.20e9	2.00e8	0	0	2.00e8
1500	9.00e8	0	0	8.50e8	2.00e8	0	0	2.00e8
2000	9.00e8	0	0	8.50e8	1.00e7	0	0	1.00e7
2500	1.00e9	0	0	1.00e9	1.00e7	0	0	1.00e7
3000	1.00e9	0	0	1.00e9	1.00e7	0	0	1.00e7
3500	1.00e9	0	0	1.00e9	1.00e7	0	0	1.00e7

Table 3 Linearized dynamic coefficents for bearing #3 & #4.

Rotating speed	k_{xx}	k_{xy}	k_{yx}	k_{yy}	r_{xx}	r_{xy}	r_{yx}	r_{yy}
300	4.00e9	–2.01e9	–2.78e7	2.00e9	5.00e7	–1.25e7	–2.00e7	2.00e7
1000	4.00e9	–2.01e9	–2.78e7	9.50e8	5.00e7	–1.25e7	–2.00e7	2.00e7
1500	4.00e9	–2.01e9	–2.78e7	8.00e8	5.00e7	–1.25e7	–2.00e7	2.00e7
2000	3.50e9	–2.01e9	–2.78e7	6.50e8	1.50e7	–7.50e6	–7.50e6	7.50e6
2500	9.00e8	–5.00e8	2.70e8	6.00e8	1.50e7	–7.50e6	–7.50e6	7.50e6
3000	7.00e8	–5.00e8	2.70e8	5.00e8	1.50e7	–7.50e6	–7.50e6	7.50e6
3500	7.00e8	–5.00e8	2.70e8	5.00e8	1.50e7	–7.50e6	–7.50e6	7.50e6

Table 4 Linearized dynamic coefficents for bearing #5 & #6.

Rotating speed	k_{xx}	k_{xy}	k_{yx}	k_{yy}	r_{xx}	r_{xy}	r_{yx}	r_{yy}
300	3.00e9	–2.23e9	–1.05e8	7.00e8	6.00e7	–1.25e7	–1.25e7	2.50e7
1000	3.00e9	–2.23e9	–1.05e8	7.00e8	6.00e7	–1.25e7	–1.25e7	2.50e7
1500	3.00e9	–2.23e9	–1.05e8	7.00e8	6.00e7	–1.25e7	–1.25e7	2.50e7
2000	1.00e9	–7.00e8	1.20e8	6.00e8	2.00e7	–1.00e7	–1.00e7	2.00e7
2500	1.00e9	–7.00e8	1.20e8	6.00e8	2.00e7	–1.00e7	–1.00e7	2.00e7
3000	1.00e9	–7.00e8	1.20e8	6.00e8	2.00e7	–1.00e7	–1.00e7	2.00e7
3500	1.00e9	–7.00e8	1.20e8	6.00e8	2.00e7	–1.00e7	–1.00e7	2.00e7

Table 5 Linearized dynamic coefficents for bearing #7.

Rotating speed	k_{xx}	k_{xy}	k_{yx}	k_{yy}	r_{xx}	r_{xy}	r_{yx}	r_{yy}
300	1.50e8	0	0	1.50e8	4.00e6	0	0	4.00e6
1000	1.50e8	0	0	1.50e8	4.00e6	0	0	4.00e6
1500	1.50e8	0	0	1.50e8	4.00e6	0	0	4.00e6
2000	8.00e7	0	0	8.00e7	2.00e6	0	0	2.00e6
2500	8.00e7	0	0	8.00e7	2.00e6	0	0	2.00e6
3000	8.00e7	0	0	8.00e7	2.00e6	0	0	2.00e6
3500	8.00e7	0	0	8.00e7	2.00e6	0	0	2.00e6

2.1.3 Modal foundation model

No previous common modal testing had been carried out on the supporting structure of this turbogenerator unit nor this task is normally performed on this type of machines, whose standard model for the foundation is made by means of pedestals. However, due to the physical characteristics of this specific foundation this approach is not satisfactory in reproducing the dynamic behaviour of the machine, which resulted rather complex in the machine speed operating range. Therefore, no reference values for the modal parameters were available.

The modal parameters of the turbogenerator foundation have been estimated using an identification technique based on the Extended Kalman Filter (EKF) described in [19,20]. At this aim the support 1x rev. vibrations measured during a run-down occurred before balancing the machine have been analysed. Moreover, the 1x rev. forces transmitted from the shaft to the foundation during the same rundown have been considered. The number of normal modes to be identified and the initial values of the natural frequencies have been defined with a preliminary analysis, of the support vibrations, in which the effects of the flexural critical speeds of the shafts have been taken into account. The complete discussion about the calculation and the reliability of the results obtained is presented in [16]. The natural frequencies and the damping ratios that have been identified are shown in table 6.

Table 6 Foundation natural frequencies and damping ratios.

	Mode n.1	Mode n.2	Mode n.3	Mode n.4	Mode n.5	Mode n.6
Natural frequency [Hz]	7.74	16.27	22.23	35.49	43.29	79.58
Damping ratio	0.02700	0.03560	0.04323	0.01760	0.03485	0.0100

Since the main interest of the study is the rotor behaviour, it is sufficient to identify the modes in the connecting nodes between the foundation and the rotor. The normal modes ψ_r have been normalised by assigning a unity value to the r-th generalised mass. Table 7 shows the foundation normal modes identified with the EKF technique; they are associated to the natural frequencies reported in table 6. Note that modes from 1 to 4 are only vertical, as shown also in figure 2, in which horizontal and vertical displacement are dimensionless since they are normalized.

Table 7 Foundation normal modes identified with the EKF technique.

Bearing	Direction	Mode n.1	Mode n.2	Mode n.3	Mode n.4	Mode n.5	Mode n.6
1	Vertical	0.0000	0.0000	–0.10622	0.0000	0.0000	6.2321
	Horizontal	0.0000	0.0000	0.0000	0.0000	0.0000	0.0000
2	Vertical	0.0000	0.0000	8.6808	0.0000	0.0000	8.6788
	Horizontal	0.0000	0.0000	0.0000	0.0000	0.0000	0.0000
3	Vertical	–0.1200	0.3305	–450.117	0.0000	0.2992	9.0155
	Horizontal	0.0000	0.0000	0.0000	0.0000	0.0000	10.8902
4	Vertical	–0.2700	–0.4002	–183.733	0.0000	–1.3000	8.7000
	Horizontal	0.0000	0.0000	0.0000	0.0000	0.0000	5.3331
5	Vertical	0.0000	0.9136	–8.2269	0.9136	2.0063	1.9000
	Horizontal	0.0000	0.0000	0.0000	0.0000	3.5117	15.6372
6	Vertical	0.0000	–1.1977	–0.2491	–1.1977	–0.9338	–4.9300
	Horizontal	0.0000	0.0000	0.0000	0.0000	0.0000	8.9195
7	Vertical	0.0000	0.0000	0.0000	0.0000	0.0000	–11.7113
	Horizontal	0.0000	0.0000	0.0000	0.0000	0.0000	–19.9892

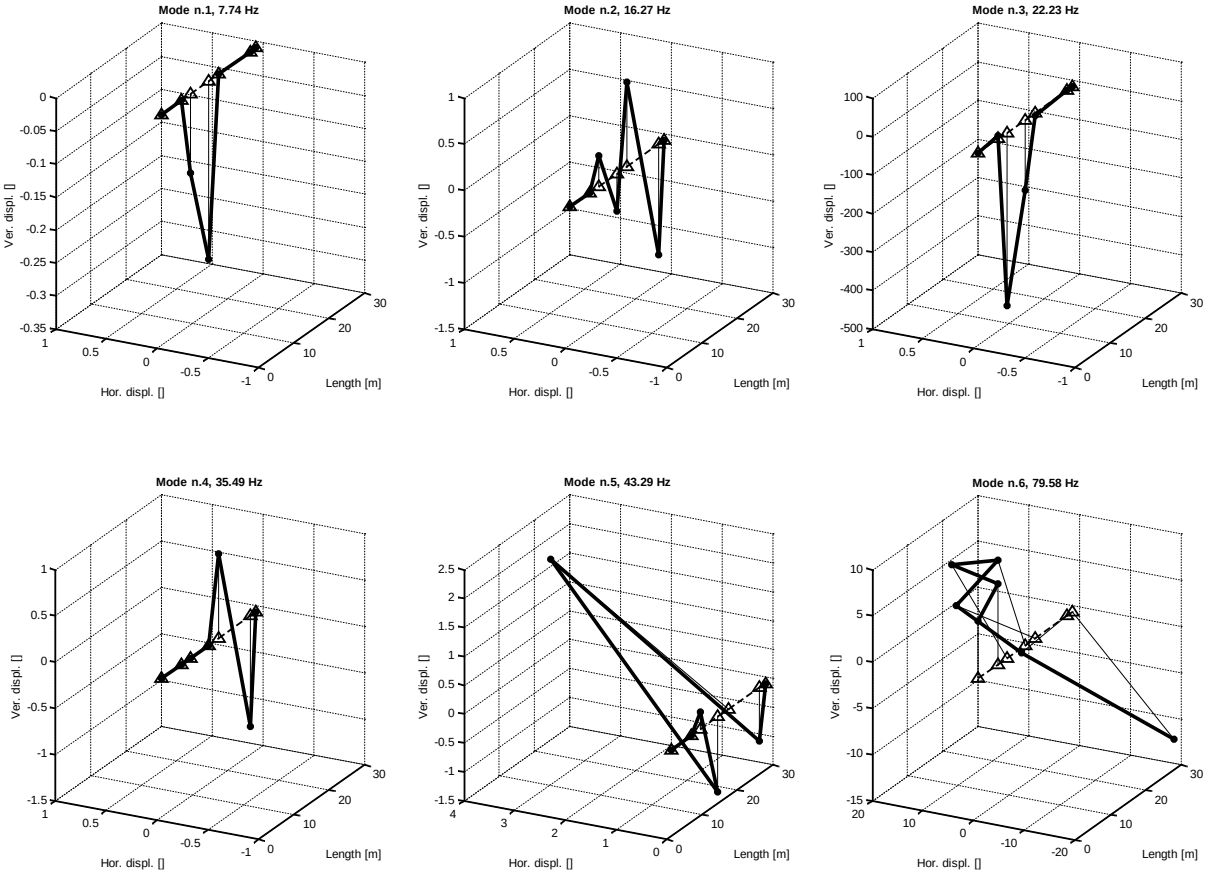

Figure 2. Foundation normal modes.

3 EXPERIMENTAL DATA

As previous mentioned, the experimental data used to obtain the additional vibrations are related to a run-down before and a run-down after a balancing on the machine. Care was taken in order to choose two run-downs in similar thermal conditions. The balancing mass was on the first balancing plane of the generator, see figure 1, that corresponds to the coupling face between the LP turbine and the generator towards the last one. The corresponding node of the model is 132. The overall amplitude of the balancing was of 0.256 kgm with a phase of −22.5° respect to the key-phasor. Due to the big inertia of the machine, the speed transients last about an hour and half and an order analysis was made, since the transient operating condition could be considered as a succession of steady-states.

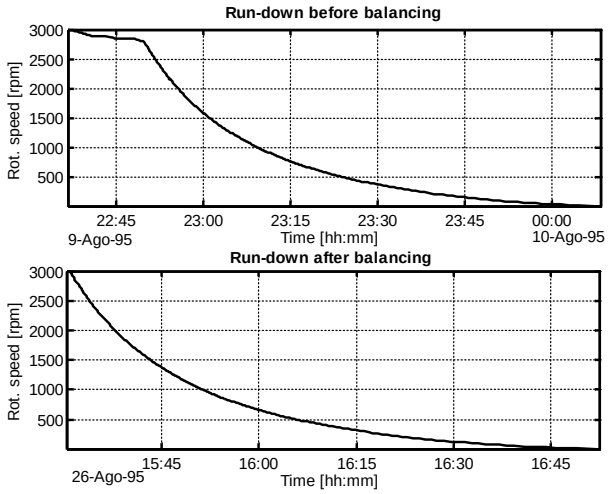

Figure 3. Run-down speed transients.

Before considering the additional vibrations that will be employed in the unbalance identification, it is interesting to evaluate the effect of the unbalance on the supporting structure vibrations measured by the velocimeters. Figure 4 shows the comparison between the support vibration in measuring plane #4 in vertical direction before and after balancing. In this case, foundation modes n. 2 (16.27 Hz, 976 rpm, see table 7) and 3 (22.23 Hz, 1334 rpm) are practically excited in the same way, while some differences are present in the higher modes.

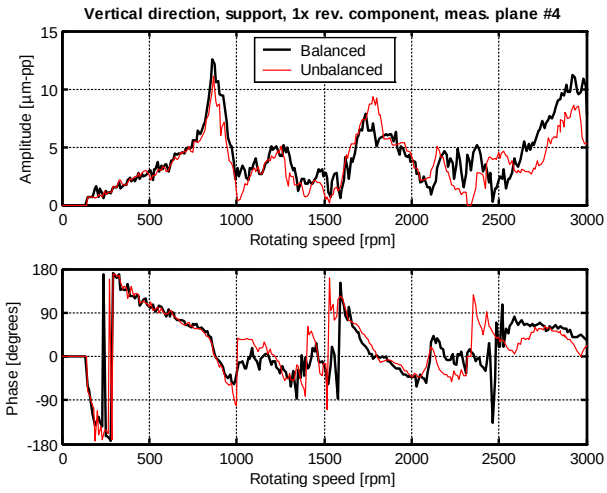

Figure 4. 1x rev. support vibrations in measuring plane #4, vertical direction. Thin line: before balancing; thick line: after balancing.

Figure 5 shows the comparison between the support vibration in measuring plane #5 in horizontal direction before and after balancing. The first mode in this direction is n. 5 (43.29 Hz, 2597 rpm, see table 7) and the unbalance effect can be appreciated.

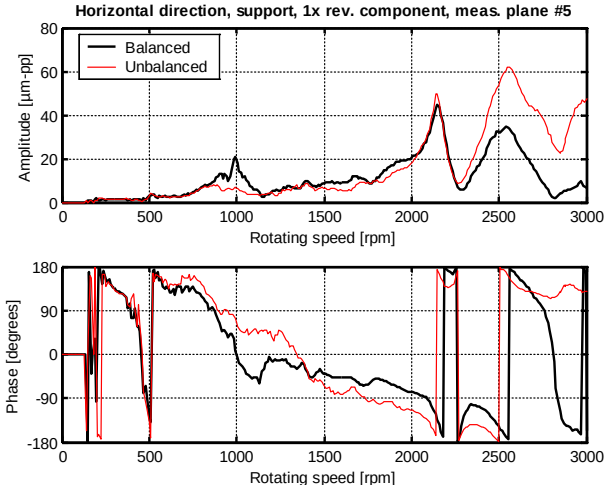

Figure 5. 1x rev. support vibrations in measuring plane #5, horizontal direction. Thin line: before balancing; thick line: after balancing.

The relative vibrations of the shaft-line measured by the proximity probes were added to the support vibrations measured by the velocimeters, obviously integrated, in order to obtain the absolute vibrations of the machine during each run-down. Finally the measures of the first run-down, that was considered as a reference case, were subtracted from those of the second run-down. The 1x rev. vibrational behaviour is shown from figure 6 to figure 12.

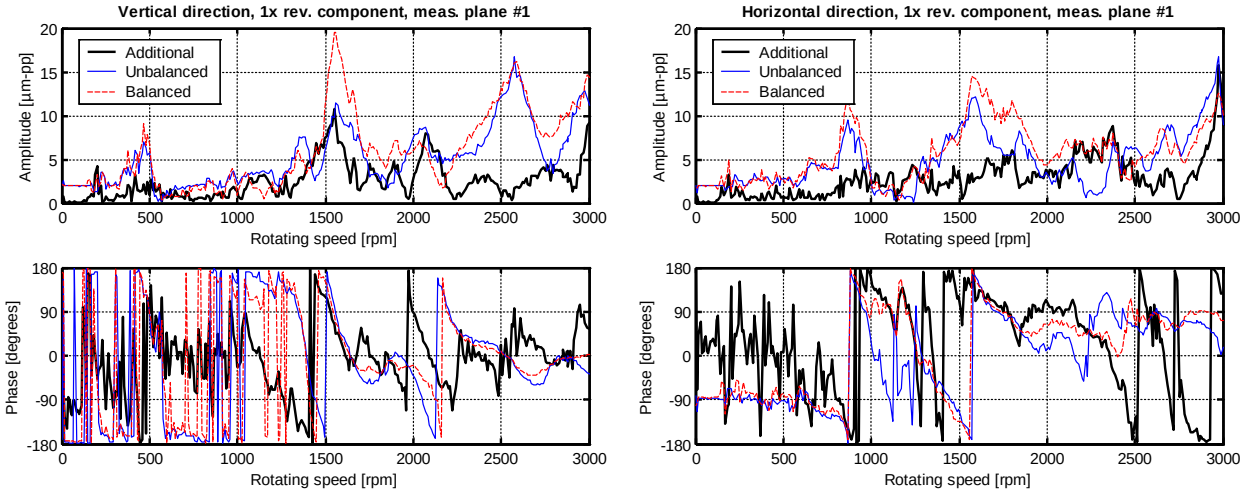

Figure 6. 1x rev. vibrations in measuring plane #1. Thin line: absolute vibrations before balancing; dashed line: absolute vibrations after balancing; thick line: additional vibrations.

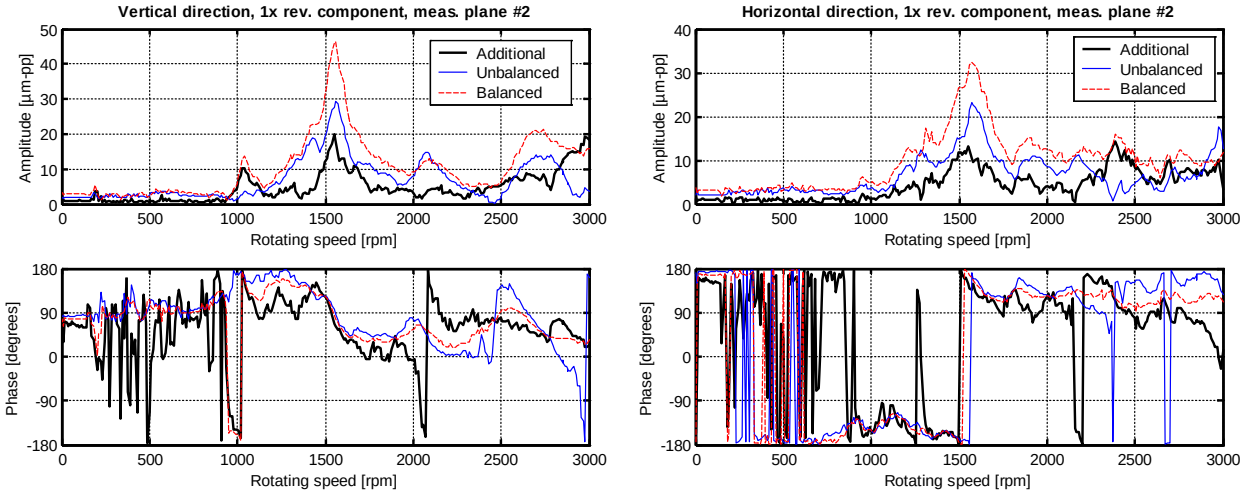

Figure 7. 1x rev. vibrations in measuring plane #2. Thin line: absolute vibrations before balancing; dashed line: absolute vibrations after balancing; thick line: additional vibrations.

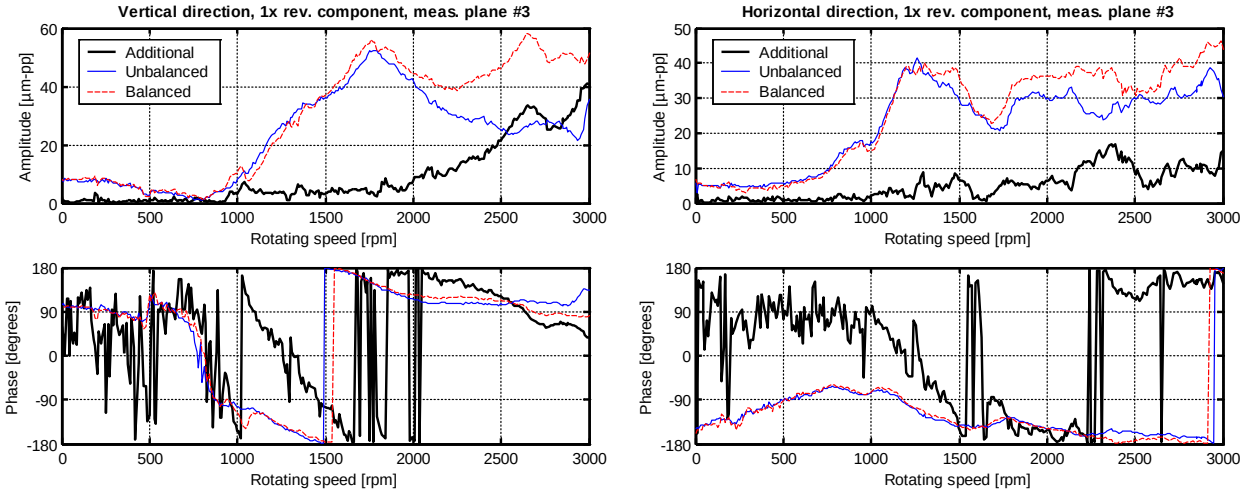

Figure 8. 1x rev. vibrations in measuring plane #3. Thin line: absolute vibrations before balancing; dashed line: absolute vibrations after balancing; thick line: additional vibrations.

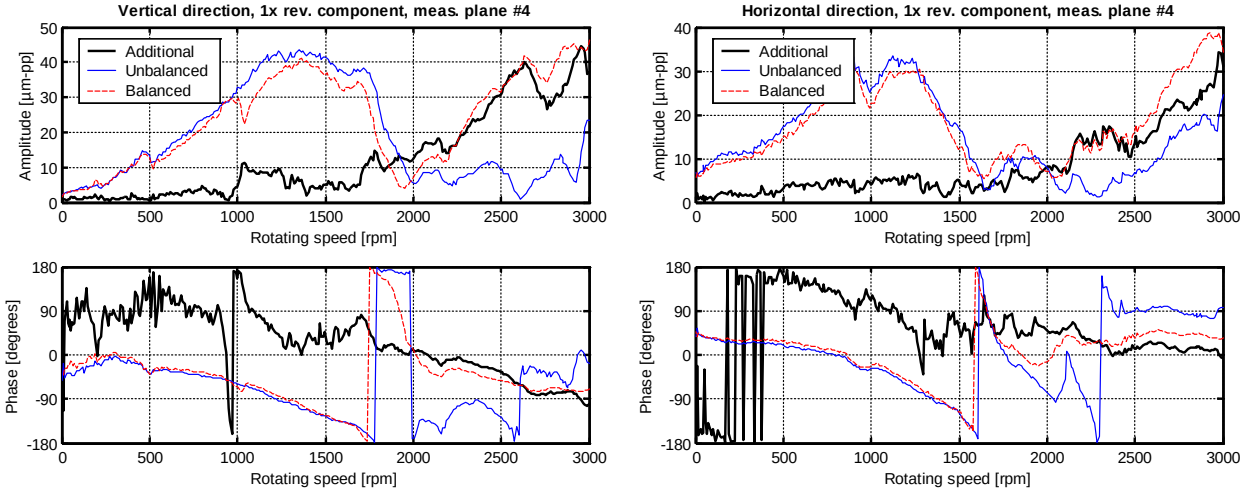

Figure 9. 1x rev. vibrations in measuring plane #4. Thin line: absolute vibrations before balancing; dashed line: absolute vibrations after balancing; thick line: additional vibrations.

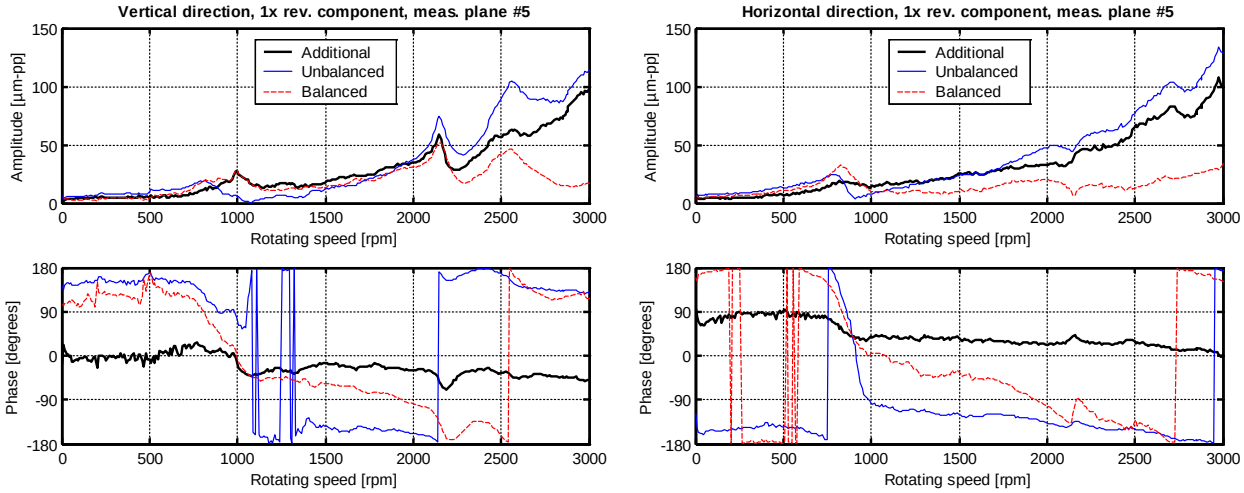

Figure 10. 1x rev. vibrations in measuring plane #5. Thin line: absolute vibrations before balancing; dashed line: absolute vibrations after balancing; thick line: additional vibrations.

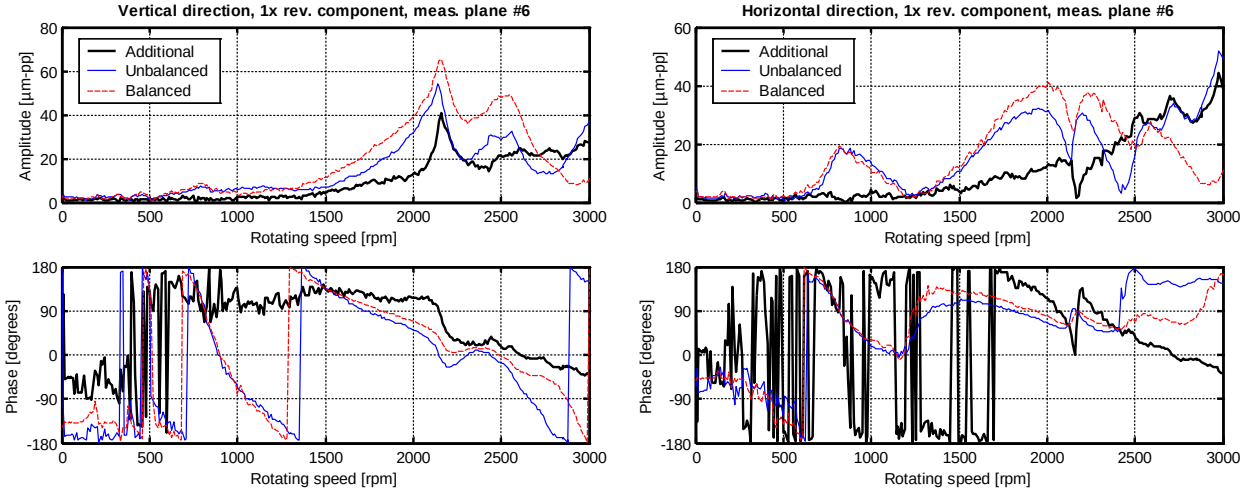

Figure 11. 1x rev. vibrations in measuring plane #6. Thin line: absolute vibrations before balancing; dashed line: absolute vibrations after balancing; thick line: additional vibrations.

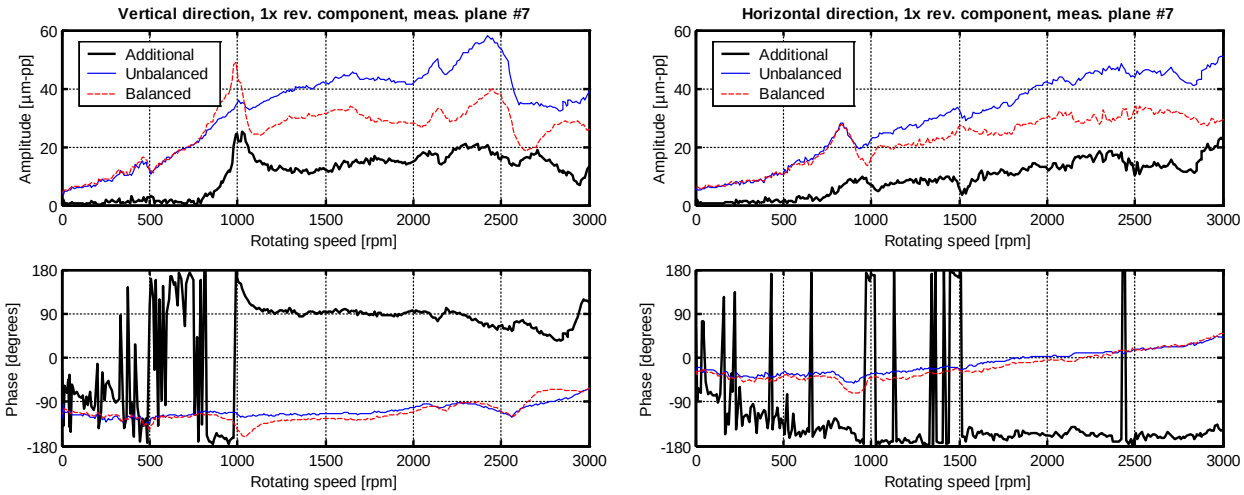

Figure 12. 1x rev. vibrations in measuring plane #7. Thin line: absolute vibrations before balancing; dashed line: absolute vibrations after balancing; thick line: additional vibrations.

The 1x rev. vibrational behaviour measured in correspondence of HP-IP turbine (figure 6 and figure 7) show that the effect of the balancing is restricted to this part of the rotor train, since the additional vibration level at high rotating speeds is low. A residual excitation of the first critical speed of the HP/IP turbine at 1560-1580 rpm, was a clear indication that a perfect thermal repeatability was not achieved among the two run-downs. These remarks are of some guidance in the set-up of the identification procedure and in the interpretation of the consequent results.

As can be expected, the effect of the balancing is more evident on the additional vibrations measured on the balancing planes of the LP turbine and of the generator (from figure 8 to figure 11), in which the parabolic trend of the vibration level is show. Also the second critical speeds in vertical direction of the LP turbine (at about 2650 rpm) and of the generator (at about 2650 rpm) are quite evident. Finally, on the measuring plane of the exciter (figure 12) the effect of the balancing is reduced, since only horizontal vibrations show a slightly increasing trend with the rotating speed.

Finally, a short discussion is made about the vibration levels at low rotating speed. Even if the measures are shown also for rotating speeds below 300 rpm, these data are not reliable at all, due to possible errors in the key-phasor signal. Therefore these experimental values will not be used for fault identification purposes and this is related also to the fact that the linarized dynamic coefficients of the bearings are not defined below 300 rpm.

The low vibration amplitude of the experimental run-downs and of the additional vibrations at low rotating speeds, in the range of 300÷700 rpm, indicates that the rotor train does not show

any permanent bow. This aspect and the previous mentioned vibration trends let the 1x rev. symptoms corresponding to those of the unbalance.

In order to evaluate the presence of non-linear effects and the fact that the condition of the speed transients are quite similar, also the 2x rev. vibrational behaviour are taken into consideration and are shown from figure 13 to figure 19. The very good repeatability of the two speed transients, which results also in the practically constant and very small additional 2x rev. vibrations in all the considered speed range, indicates the absence of non-linear effects and that there are not symptoms of faults with 2x rev. characteristic such as cracks, journal bearing ovalization or stiffness asymmetry, being the last not very uncommon in two poles generators, as the considered in this rotor train, due to their construction.

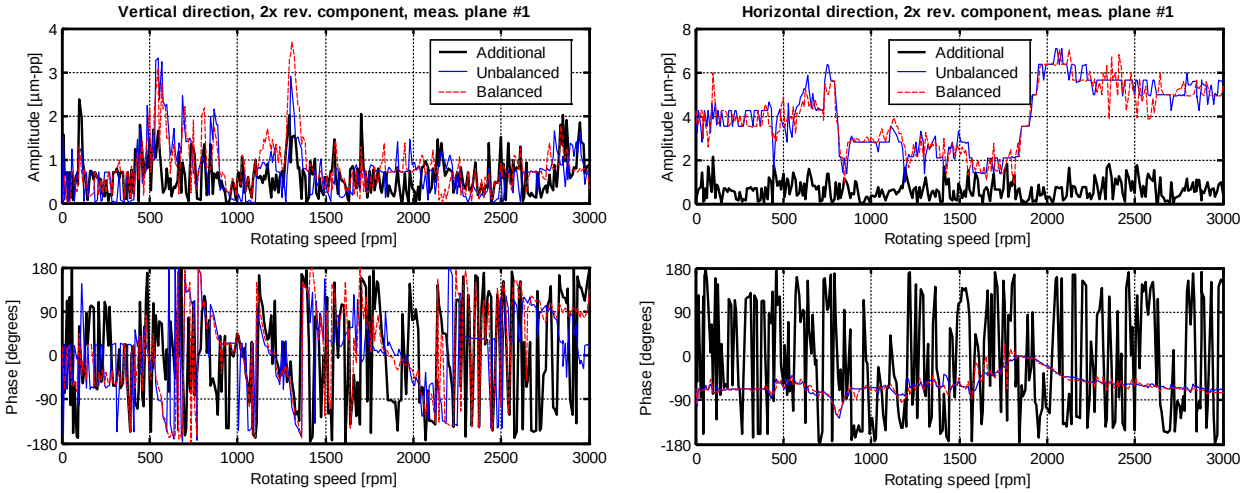

Figure 13. 2x rev. vibrations in measuring plane #1. Thin line: absolute vibrations before balancing; dashed line: absolute vibrations after balancing; thick line: additional vibrations.

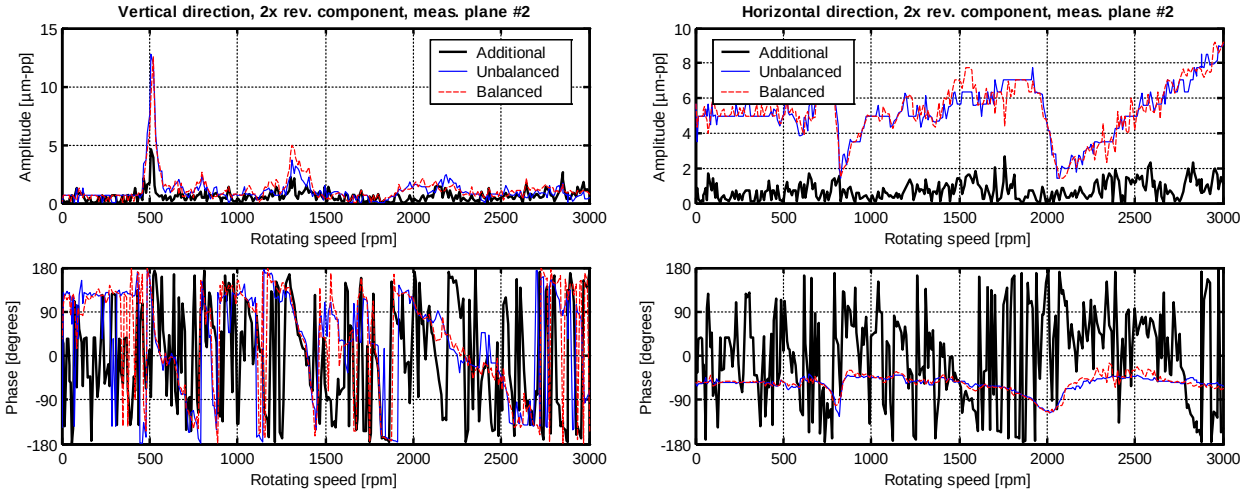

Figure 14. 2x rev. vibrations in measuring plane #2. Thin line: absolute vibrations before balancing; dashed line: absolute vibrations after balancing; thick line: additional vibrations.

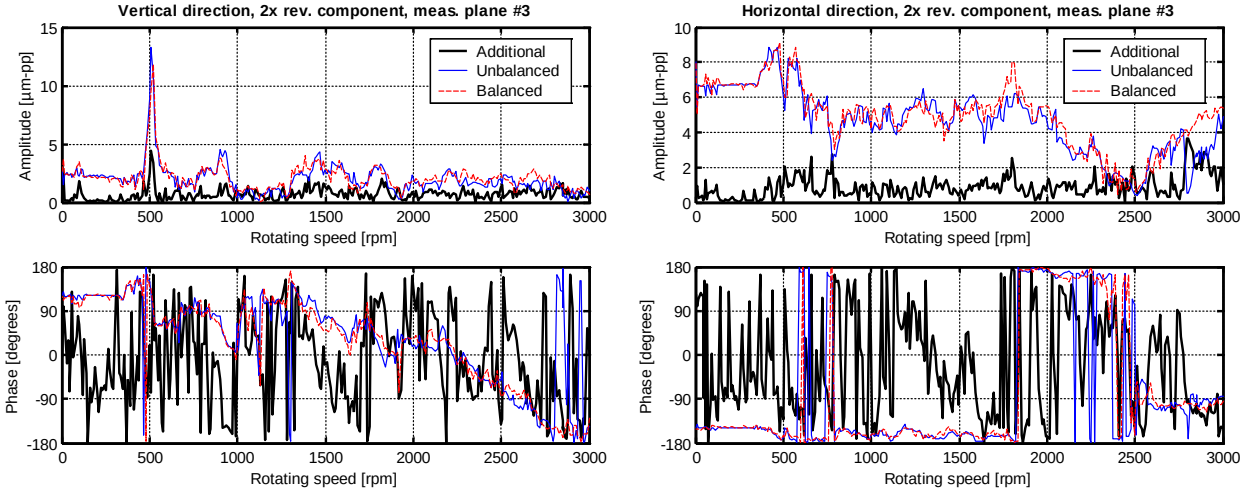

Figure 15. 2x rev. vibrations in measuring plane #3. Thin line: absolute vibrations before balancing; dashed line: absolute vibrations after balancing; thick line: additional vibrations.

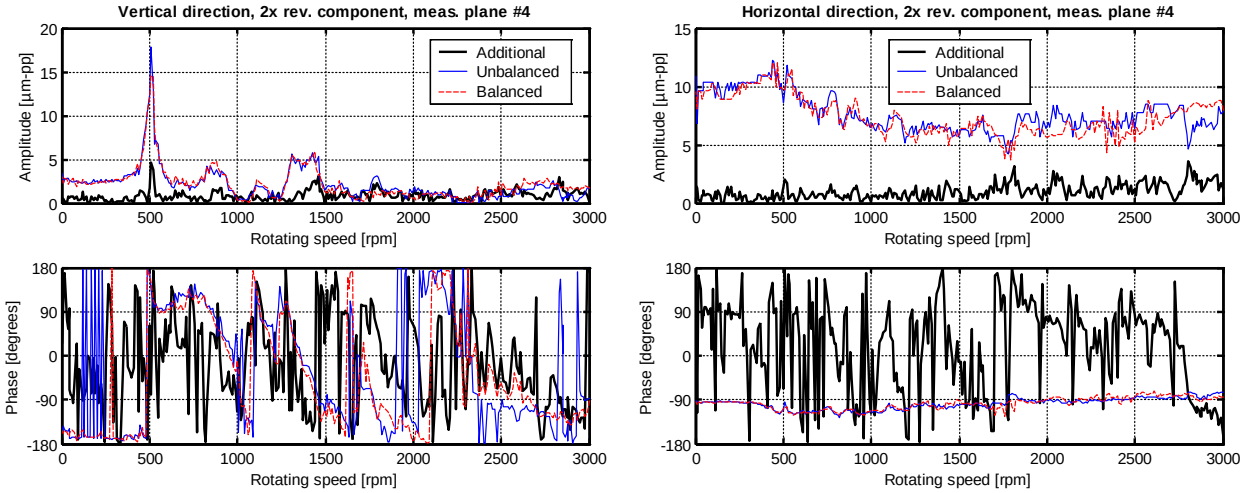

Figure 16. 2x rev. vibrations in measuring plane #4. Thin line: absolute vibrations before balancing; dashed line: absolute vibrations after balancing; thick line: additional vibrations.

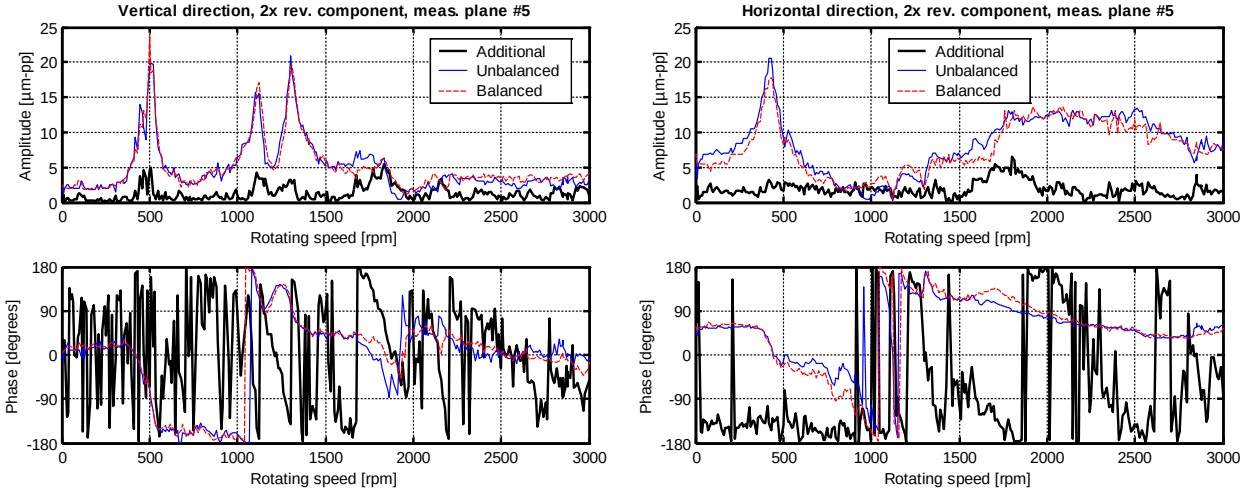

Figure 17. 2x rev. vibrations in measuring plane #5. Thin line: absolute vibrations before balancing; dashed line: absolute vibrations after balancing; thick line: additional vibrations.

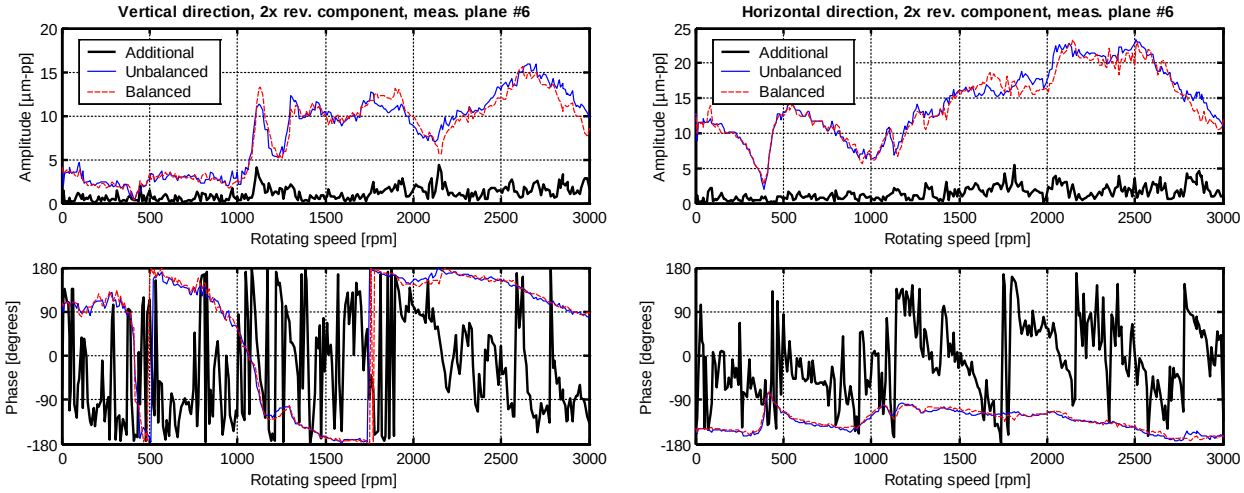

Figure 18. 2x rev. vibrations in measuring plane #6. Thin line: absolute vibrations before balancing; dashed line: absolute vibrations after balancing; thick line: additional vibrations.

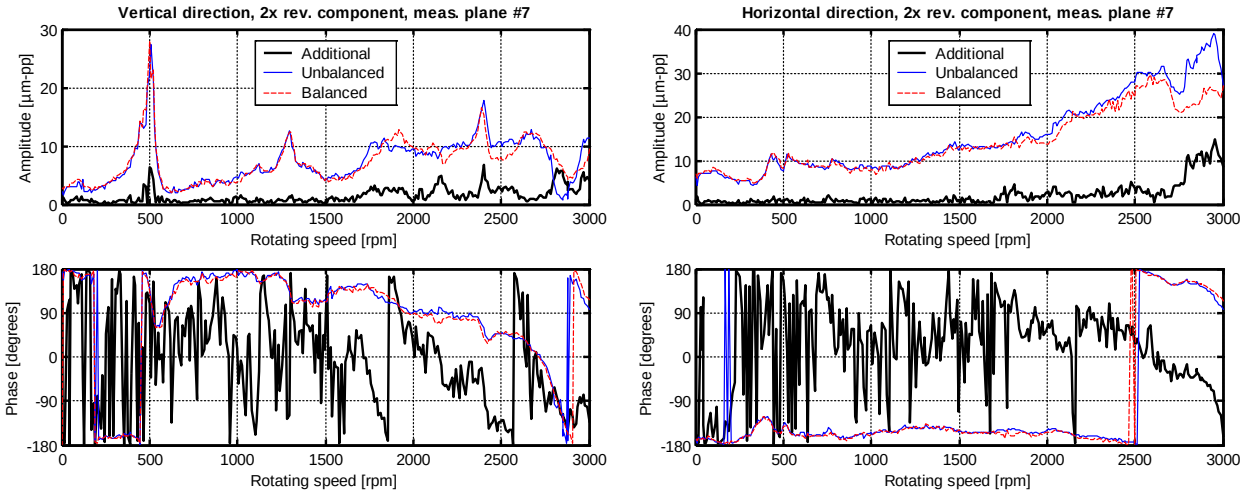

Figure 19. 2x rev. vibrations in measuring plane #7. Thin line: absolute vibrations before balancing; dashed line: absolute vibrations after balancing; thick line: additional vibrations.

4 UNBALANCE IDENTIFICATION

As it follows from the identification technique described in detail in the first part of the paper, the results obtained depend on the selected subset of the rotating speeds at which the additional vibration are considered and on the weights assigned to each measure. Both these aspects are now taken into consideration. In regards to the subset of the rotating speeds three different sets are used:

- the first set, $\mathbf{V}_1$ considers the additional vibrations corresponding to the rotating speeds of 2000, 2250, 2500, 2750 and 3000 rpm; this set is that normally chosen by people of the control room of the power plant. It reflects their opinion, not necessarily shared by the authors, that the model and the measured vibrations are reliable only over 2000 rpm. The advantage of this set is its reduced order, but due to this fact it can miss important information about the vibrational behaviour of the machine;
- the second set, $\mathbf{V}_2$, considers the entire all the data and extracts the additional vibration corresponding to each 10 measures. The corresponding rotating speeds are approximately equally spaced of 100 rpm in the range from 0 to 3000 rpm. This way, the complete vibrational behaviour of the machine is sampled and the order of the least square problem is not huge, but in certain ranges neither the model nor the measures (typically in resonance or at low rotating speed) could be reliable;
- the third set, $\mathbf{V}_3$, considers all the data. The order of the problem is huge and the computational time is large, but the effect of the presence of biased measures or outliers is minimized.

The criteria used to select the weights of the weighted last squares identification method reflect the analysis of the vibration data presented in this chapter:

- the first set of weights $\mathbf{W}_1$ assign unitary weight to each measure. This way the fault acts on the entire machine even if on such large machine the effects are normally more local and are more evident in the measuring planes close to the fault position. Anyway this choice, in which the least squares is actually not weighted, reflects a not identification expert attitude;
- the second set of weights $\mathbf{W}_2$ assign unitary weight to the measures corresponding to the measuring planes of the LP turbine and of the generator, while the weight of the measuring planes of HP-IP turbine are equal to 0.1. This set reflects the observations made about the 1x rev. additional vibrations at the beginning of this chapter;
- the third set of weights $\mathbf{W}_3$ endow the measuring planes close to bearings #4 and #5 by assigning unitary weight to their measures, assign weight equal to 0.5 to measuring planes #3 and #6 and equal to 0.1 to the others. This way the effect of the fault is considered as local.

The use of the presented technique allows the relative residuals to be calculated and, in case of a fault, to obtain a graphical representation such as that shown in figure 20 in case of sets $\mathbf{V}_2$ and $\mathbf{W}_1$.

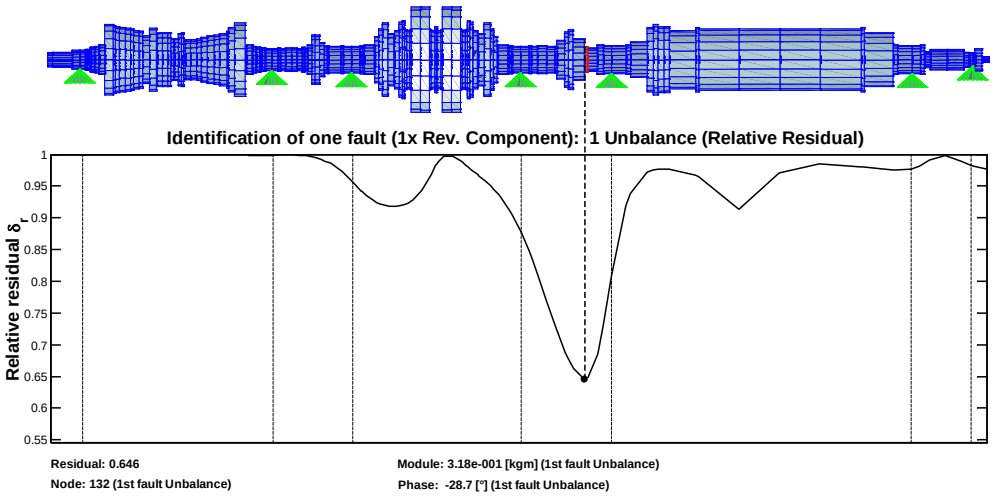

Figure 20. Calculation of the relative residual for all the nodes of the shaft line, localization of the fault.

The minimum of the relative residual curve indicates the node *s*-th in which the fault, the unbalance, is most probably localised, while the corresponding values of the amplitude and phase of:

$$\mathbf{A}^{(s)} = \left(\left[\hat{\mathbf{X}}_{\mathrm{B}n} \right]^{\mathrm{T}} \left[\hat{\mathbf{X}}_{\mathrm{B}n} \right] \right)^{-1} \left[\hat{\mathbf{X}}_{\mathrm{B}n} \right]^{\mathrm{T}} \left[\mathbf{W} \right] \mathbf{X}_{\mathrm{B}mn} \tag{1}$$

give the estimate of the fault severity. It can be observed that the minimum of the relative residual curve in correspondence of the fault position is very clearly defined with respect to the values in any other position along the shaft-line. In the case shown the position of the unbalance is correctly identified (see figure 1), the module is slightly overestimated (0.318 vs. 0.256 kgm) and the phase has a very good fitting (–28.7° vs. –22.5°). The minimum value of the relative residual is 0.646 can be deemed as good taking into consideration that the data are actually experimental, i.e. the identified unbalance gives a rather good explanation of the additional vibrations. This fact can be verified if the experimental additional vibration are compared with the simulated vibration calculated by means of the fully assembled model of the machine and the identified unbalance as shown in figure 21 and figure 22 for the generator measuring planes #5 and #6 only for conciseness.

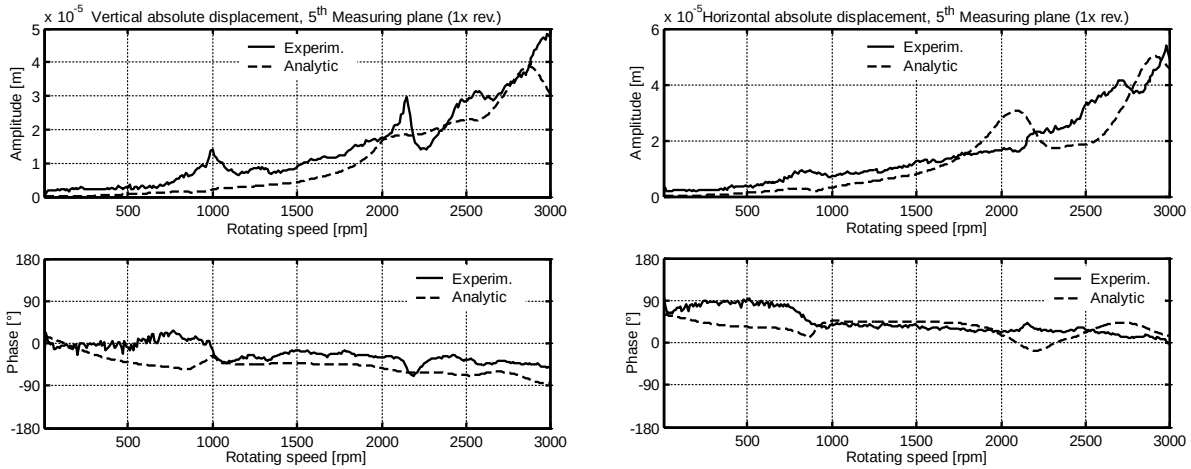

Figure 21. Comparison between experimental and calculated vibrations, #5 measuring plane.

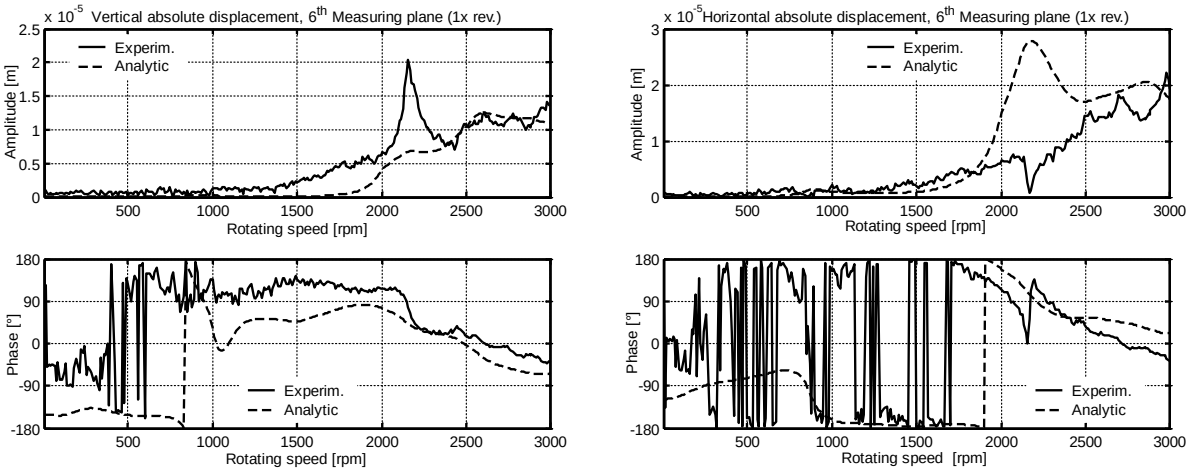

Figure 22. Comparison between experimental and calculated vibrations, #6 measuring plane.

The complete results, using the selected sets of additional vibrations and weights are reported in table 8, table 9 and table 10, in which also the percentage errors are reported. For the phase only, a ±100% error indicates a phase error of ±180°, while the error on the position, is calculated with respect of the rotor length.

The results are always remarkable in regards to the unbalance position. This is a most important piece of information from an engineering viewpoint, because it also addresses the possible source of the fault. The phase angle identification is also remarkably good in all cases and of sure interest for the vibration specialist. Larger errors, up to 40%, are found in the amplitude identification, with an average error of 27.3% among all the tests, but it is worth saying that also this result is certainly more than acceptable.

The use of set $\mathbf{W}_3$, independently of the speed set, determines the lowest values of the residual, but not necessarily the most precise estimation of the unbalance position and module. A better selection of the weights can be determined by means of the regression diagnostics or residual analysis techniques discussed in [21,22], in order to increase the accuracy of the fault parameter estimate.

Due to the good quality of the experimental data, the results obtained with the different speed sets are very similar. Finally, it is worth to remember that these good results are obtained despite the fact that the bearing models are not fine tuned and the rotor model is the standard one, common to all the machines of this type.

Table 8. Unbalance identification results using data corresponding to speed set $\mathbf{V}_1$.

Speed set $\mathbf{V}_1$	Residual	Node	Error on location	Module [kgm]	Error on module	Phase [°]	Error on phase
Weight set $\mathbf{W}_1$	0.646	132	0%	0.317	24%	–36.8	–8%
Weight set $\mathbf{W}_2$	0.646	132	0%	0.321	25%	–36.0	–8%
Weight set $\mathbf{W}_3$	0.558	133	0.35%	0.359	40%	–35.7	–7%

Table 9. Unbalance identification results using data corresponding to speed set $\mathbf{V}_2$.

Speed set $\mathbf{V}_2$	Residual	Node	Error on location	Module [kgm]	Error on module	Phase [°]	Error on phase
Weight set $\mathbf{W}_1$	0.646	132	0%	0.318	24%	–28.7	–3%
Weight set $\mathbf{W}_2$	0.641	132	0%	0.318	24%	–28.8	–4%
Weight set $\mathbf{W}_3$	0.546	133	0.35%	0.354	38%	–27.9	–3%

Table 10. Unbalance identification results using data corresponding to speed set $\mathbf{V}_3$.

Speed set $\mathbf{V}_3$	Residual	Node	Error on location	Module [kgm]	Error on module	Phase [°]	Error on phase
Weight set $\mathbf{W}_1$	0.715	134	1.40%	0.186	–27%	–18.6	2%
Weight set $\mathbf{W}_2$	0.711	134	1.40%	0.186	–27%	–18.5	2%
Weight set $\mathbf{W}_3$	0.649	134	1.40%	0.213	–17%	–16.5	3%

4.1 Robustness of the unbalance identification in regards to faults with similar symptoms

The last check on the robustness of the identification is performed by considering other possible faults that have similar symptoms and verifying that the unbalance is the most likely fault, i.e. it has the lowest value of the relative residual. Therefore other faults that present a 1x rev. symptom are considered, whose models are described in detail in [12]:

- the “local” bow, that can represent for instance the effect of a rub, which determines an asymmetric local thermal distribution. In this case the local bow is intended as affecting an element of the rotor only.
- the “extended” bow, which is the actual shaft bow, that is considered as affecting a rotor part limited by two bearings.
- the rigid coupling misalignment, both in angular and radial (also known as parallel, see [23-25]) direction; obviously in the considered machine, this fault has two possible location only.

The results are shown in table 11, table 12 and table 13 using the same sets of speeds and weights of the unbalance identification. Since in this case the task is to check that the unbalance is the most likely fault, there is not interest in reporting also the eventual position or magnitude of the other fault types, even if they are also obtained by means of the identification technique.

Table 11. Residual values of identified faults having 1x rev. symptom, corresponding to speed set $\mathbf{V_1}$.

Speed set $\mathbf{V_1}$	Unbalance	Local bow	Extended bow	Coupling misalignment
Weight set $\mathbf{W_1}$	0.646	0.665	0.780	0.671
Weight set $\mathbf{W_2}$	0.646	0.679	0.777	0.678
Weight set $\mathbf{W_3}$	0.558	0.593	0.643	0.584

Table 12. Residual values of identified faults having 1x rev. symptom, corresponding to speed set $\mathbf{V_2}$.

Speed set $\mathbf{V_2}$	Unbalance	Local bow	Extended bow	Coupling misalignment
Weight set $\mathbf{W_1}$	0.646	0.749	0.848	0.729
Weight set $\mathbf{W_2}$	0.641	0.743	0.843	0.723
Weight set $\mathbf{W_3}$	0.546	0.640	0.758	0.622

Table 13. Residual values of identified faults having 1x rev. symptom, corresponding to speed set $\mathbf{V_3}$.

Speed set $\mathbf{V_3}$	Unbalance	Local bow	Extended bow	Coupling misalignment
Weight set $\mathbf{W_1}$	0.715	0.799	0.802	0.755
Weight set $\mathbf{W_2}$	0.711	0.793	0.789	0.748
Weight set $\mathbf{W_3}$	0.649	0.799	0.716	0.691

Of course, also in consideration of the peculiar location of the unbalance next to the LP/generator coupling, dramatic differences in the residual values between unbalance, local bow and coupling errors could not be expected in this particular case.

In all the considered cases, the relative residual of the unbalance is the lowest, confirming that the identified fault is the most likely one and that the method is robust in regards to of the symptoms. Moreover, if the difference between the residual values can be assumed as an approximate measure of uncertainty in the identification of the type of the fault, the use of small set of experimental values (set $\mathbf{V}_1$) gives the most uncertain results, while the uncertainty tends to reduce and to settle down with large sets ($\mathbf{V}_2$ and $\mathbf{V}_3$).

5 CONCLUSIONS

The theoretical developments, presented in first part of the paper about the use of a modal foundation in a model based identification technique in frequency domain, were validated by means of data coming from trim balancing tests on a large steam turbogenerator rotor operating in a power plant. The experimental data are presented and discussed. The results demonstrate not only a high precision and robustness of the proposed approach in the localization of the fault position along the shaft-line, but also a good approximation in the identification of amplitude and phase of the fault. Moreover the ability of the method to single out the correct type of fault among others with similar symptoms is proven.

REFERENCES

[1] Isermann R. and Ballé P., “Trends in the Application of Model-based Fault Detection and Diagnosis of Technical Process”, Control Engineering Practice (1997) 5(5), 709-719.

[2] Hellmann D-H., “Early fault detection – an overview –”, *ISROMAC-9 Conference*, February 2002, Honolulu, Hawaii, 1-5.

[3] White M.F. and Jecmenica M., “Fault diagnosis using a fault matrix incorporating fuzzy logic”, *12th International Congress on Condition Monitoring and Diagnostic Engineering Management-COMADEM 99*, July 1999, Sunderland, 441-450.

[4] Kirk G.R. and Guo Z., “Expert system source identification of excessive vibration”, International Journal of Rotating Machinery (2003) 9(2), 63-79.

[5] Arnaiz A. and Arzamendi J., “Adaptive diagnostics systems by means of Bayesian network”, *Condition Monitoring and Diagnostic Engineering Management-COMADEM 2003*, August 2003, Växjö, 155-164.

[6] Vyas N.S. and Satishkumar D., “Artificial neural network design for fault identification in a rotor-bearing system”, *Mechanism and Machine Theory* (2001) 36, 157-175.

[7] Lucifredi A., Magnetto A. and Silvestri P., "Experimental validation of an original software package based on chaos theory for monitoring and diagnostics of rotating machinery", *IFToMM-6th International Conference on Rotor Dynamics*, September - October 2002, Sydney, Australia, 257-266.

[8] Mayes I. and Penny J.E.T., "Model based diagnostics of fault in rotating machines", *12th International Congress on Condition Monitoring and Diagnostic Engineering Management-COMADEM 99*, July 1999, Sunderland, 431-440.

[9] Platz R., Markert R. and Seidler M., "Validation of online diagnostics of malfunctions in rotor systems", IMechE paper C576-025, *7th Int. Conf. on Vibrations in Rotating Machinery*, September 2000, University of Nottingham, 581-590.

[10] Kiciński J., "Model-based diagnostics in 200MW turbosets" *Survelliance 4 – Acoustical and Vibratory Surveillance Methods and Diagnostic Techniques*, October 2001, Compiègne, France, 365-377.

[11] Bachschmid N., Pennacchi P., Vania A., Zanetta G.A. and Gregori L., "Case Studies of Fault Identification in Power Plant Large Rotating Machinery", *IFToMM-6th International Conference on Rotor Dynamics*, September - October 2002, Sydney, Australia, 191-200.

[12] Bachschmid N., Pennacchi P. and Vania A., "Identification of multiple faults in rotor systems", Journal of Sound and Vibration (2002) 254(2), 327-366.

[13] Konishi T., Allaire P. and Untaroiu C., "Modal analysis of a large turbine-generator system with foundation effects", *IFToMM-6th International Conference on Rotor Dynamics*, September - October 2002, Sydney, Australia, 846-853.

[14] Feng N. and Hahn E.J., "Numerical evaluation of an identification technique for flexibly supported rigid turbomachinery foundations", *IFToMM-6th International Conference on Rotor Dynamics*, September - October 2002, Sydney, Australia, 854-861.

[15] Smart M., Friswell M.I., Lees A.W. and Prells U. "Estimating turbogenerator foundation parameters", *Proc Instn Mech Engrs* (1998) 212 part C, 635-665.

[16] Vania A., "On the identification of the foundation of a large turbogenerator unit by the analysis of transient vibrations", IMechE paper C576-076, *7th Int. Conf. on Vibrations in Rotating Machinery*, September 2000, University of Nottingham, UK, 571-580.

[17] Provasi R. and Zanetta G.A., "DYNARO-Dynamic analysis of rotors-User Manual", *ENEL-SRI-PDM-DIM* 98-11 01.09.1998.

[18] Someya T., Journal-Bearing Databook, Springer-Verlag, 1989.

[19] Vania A., Bachschmid N., Zanetta G.A. and Provasi R., "Task 2 - Model the rotor – bearing – foundation system, Subtask 2.3.3 – Identify turbogenerator foundation", Brite EuRam Project BE95-2015 (1999), 1-64.

[20] Provasi R., Zanetta G.A. and Vania A., "The extended Kalman filter in the frequency domain for the identification of mechanical structures excited by sinusoidal multiple inputs", Mechanical Systems and Signal Processing (2000) 14(3), 327-341.

[21] Vania A. and Pennacchi P., "Experimental and theoretical application of fault identification measures of accuracy in rotating machine diagnostics", Mechanical Systems and Signal Processing, (2004) 18(2), 329-352.

[22] Zhang Z., "Parameter estimation techniques: a tutorial with application to conic fitting", Image and Vision Computing (1997) 15, 59-76.

[23] Rao J.S. and Chawla A., "Analytical and experimental investigation on misaligned rotors", *ISROMAC-9 Conference*, February 2002, Honolulu, Hawaii, 1-8.

[24] Sekhar A.S. and Prabhu B.S., "Effects of Coupling Misalignment on Vibrations of Rotating Machinery", Journal of Sound and Vibration, 1995, 185(4), 655-671.

[25] Prabhakar S., Sekhar A.S. and Mohanty A.R., “Vibration Analysis of a Misaligned Rotor-Coupling-Bearing system passing through the critical speed”, *Proc Instn Mech Engrs* (2001) 215 part C, 1417-1428.